Chemistry of fracture-filling raised ridges in Yellowknife Bay, Gale Crater: Window into past aqueous activity and habitability on Mars

Richard J. Leveille, John Bridges, Roger C. Wiens, Nicolas Mangold, Agnes Cousin, Nina Lanza, Olivier Forni, Ann Ollila, John Grotzinger, Samuel Clegg, et al.

AGU PUBLICATIONS

JGR

Journal of Geophysical Research: Planets

RESEARCH ARTICLE
10.1002/2014JE004620

Special Section:
Results from the first 360 Sols of the Mars Science Laboratory Mission: Bradbury Landing through Yellowknife Bay

Key Points:
- Raised ridges were investigated by the Curiosity rover in the Sheepbed mudstone
- Their chemistry shows an enrichment in Mg
- Composition reveals a cement stratigraphy

Supporting Information:
- Table S1

Correspondence to:
R. J. Léveillé,
rich.leveille@gmail.com

Citation:
Léveillé, R. J., et al. (2014), Chemistry of fracture-filling raised ridges in Yellowknife Bay, Gale Crater: Window into past aqueous activity and habitability on Mars, *J. Geophys. Res. Planets*, *119*, 2398–2415, doi:10.1002/2014JE004620.

Received 31 JAN 2014
Accepted 16 JUL 2014
Accepted article online 18 JUL 2014
Published online 26 NOV 2014

Chemistry of fracture-filling raised ridges in Yellowknife Bay, Gale Crater: Window into past aqueous activity and habitability on Mars

Richard J. Léveillé[1,2], John Bridges[3], Roger C. Wiens[4], Nicolas Mangold[5], Agnes Cousin[4], Nina Lanza[4], Olivier Forni[6,7], Ann Ollila[8], John Grotzinger[9], Samuel Clegg[4], Kirsten Siebach[9], Gilles Berger[6,7], Ben Clark[10], Cécile Fabre[11], Ryan Anderson[12], Olivier Gasnault[6,7], Diana Blaney[13], Lauren Deflores[13], Laurie Leshin[14], Sylvestre Maurice[6,7], and Horton Newsom[8]

[1]Canadian Space Agency, Saint-Hubert, Quebec, Canada, [2]Department of Natural Resource Sciences, McGill University, Montreal, Quebec, Canada, [3]Space Research Centre, Department of Physics and Astronomy, University of Leicester, Leicester, UK, [4]Los Alamos National Laboratory, Los Alamos, New Mexico, USA, [5]Laboratoire de Planétologie et Géodynamique de Nantes, Université de Nantes, Nantes, France, [6]Université de Toulouse, UPS-OMP, IRAP, Toulouse, France, [7]CNRS, IRAP, Toulouse, France, [8]Institute of Meteoritics, University of New Mexico, Albuquerque, New Mexico, USA, [9]Laboratoire de Planétologie et Géodynamique de Nantes, California Institute of Technology, Pasadena, California, USA, [10]Space Science Institute, Boulder, Colorado, USA, [11]Université de Lorraine, GeoRessources UMR CNRS, Nancy, France, [12]United States Geological Survey, Flagstaff, Arizona, USA, [13]Jet Propulsion Laboratory, Pasadena, California, USA, [14]Rensselaer Polytechnic Institute, Troy, New York, USA

Abstract The ChemCam instrument package on the Curiosity rover was used to characterize distinctive raised ridges in the Sheepbed mudstone, Yellowknife Bay formation, Gale Crater. The multilayered, fracture-filling ridges are more resistant to erosion than the Sheepbed mudstone rock in which they occur. The bulk average composition of the raised ridges is enriched in MgO by 1.2–1.7 times (average of 8.3–11.4 wt %; single-shot maximum of 17.0 wt %) over that of the mudstone. Al_2O_3 is anticorrelated with MgO, while Li is somewhat enriched where MgO is highest. Some ridges show a variation in composition with different layers on a submillimeter scale. In particular, the McGrath target shows similar high-MgO resistant outer layers and a low-MgO, less resistant inner layer. This is consistent with the interpretation that the raised ridges are isopachous fracture-filling cements with a stratigraphy that likely reveals changes in fluid composition or depositional conditions over time. Overall, the average composition of the raised ridges is close to that of a Mg- and Fe-rich smectite, or saponite, which may also be the main clay mineral constituent of the host mudstone. These analyses provide evidence of diagenesis and aqueous activity in the early postdepositional history of the Yellowknife Bay formation, consistent with a low salinity to brackish fluid at near-neutral or slightly alkaline pH. The fluids that circulated through the fractures likely interacted with the Sheepbed mudstone and (or) other stratigraphically adjacent rock units of basaltic composition and leached Mg from them preferentially.

1. Introduction

The Curiosity rover successfully landed in Gale Crater on 5 August 2012. Since then, it has been exploring a part of the crater floor in search of signs of past or present habitable conditions. The rover has a science payload consisting of 10 instruments, including CheMin, the first planetary X-ray diffraction instrument. In addition, the ChemCam instrument package includes the first laser-induced breakdown spectroscopy (LIBS) instrument to operate on another planet. It combines a mast-mounted optical head, which includes the laser and sensor optics as well as a remote microscopic imager (RMI), and a body-mounted unit containing the three spectrometers and electronics [*Maurice et al.*, 2012; *Wiens et al.*, 2012]. *Williams et al.* [2013] demonstrated the use of ChemCam for investigating conglomerates, including the detection of hydrogen, near the rover's landing site in Gale Crater. *Meslin et al.* [2013] also used ChemCam to probe Martian soil and dust, and they showed evidence for chemical variability at the submillimeter scale. In the latter case, the small sampling area of the ChemCam laser was uniquely suited to identify mixing trends in materials of different grain sizes.

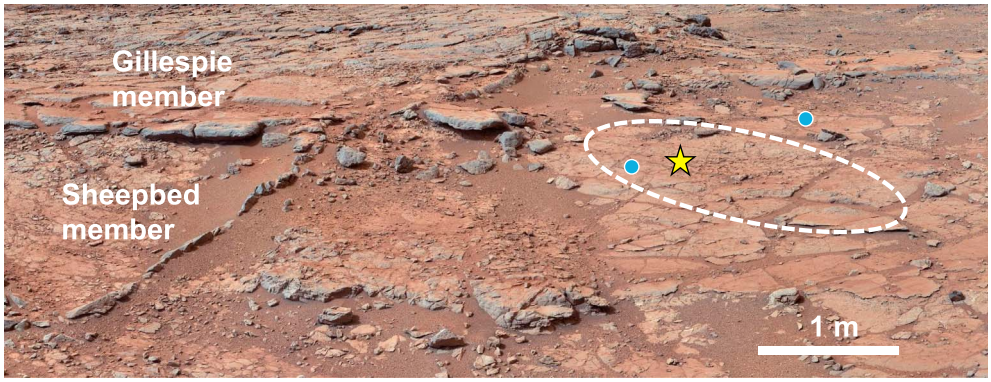

Figure 1. Partial Mastcam M100 mosaic (sol 137 + sol 138 + sol 141) showing the contact between the Sheepbed and Gillespie members of the Yellowknife Bay formation. The dotted oval highlights a cluster of raised ridges, which includes the McGrath and John Klein targets (yellow star). These are located between the two drill holes (blue circles). The vein-like raised ridges are concentrated in the Sheepbed member.

Sedimentary features, including cements, concretions, nodules, mineral vugs, and veins, have been investigated with the Mars Exploration Rovers *Opportunity* and *Spirit*, typically revealing a complex diagenetic history [*Squyres et al*., 2004, 2012; *McLennan et al*., 2005; *Knoll et al*., 2008; *Arvidson et al*., 2014]. More recently, the *Curiosity* rover investigated late-stage diagenetic Ca-S-rich veins, as well as hollow and filled nodules (concretions) in fine-grained sedimentary rocks within Gale Crater [*Grotzinger et al*., 2014; *McLennan et al*., 2014; *Nachon et al*., 2014; *Stack et al*., 2014]. The ChemCam instrument is particularly well suited for rapid and remote analyses and high-resolution imaging of such features. Here we demonstrate the use of the ChemCam instrument for fine-scale, three-dimensional chemical analyses of complex, multilayered, early diagenetic fracture-filling cements in the Yellowknife Bay formation of Gale Crater, Mars. These "raised ridges" were first described in *Grotzinger et al*. [2014] and *McLennan et al*. [2014], but we provide here a greatly expanded data set and analysis of ChemCam compositional results, including depth profiles, which, when combined with surface rasters, effectively provide three-dimensional analyses of these small-scale features.

The raised ridges consist of narrow (<1 mm to 6 mm in total width; several centimeters in length), curvilinear ridges that have differentially weathered relative to the surrounding rock, creating a raised relief of several millimeters [*Siebach et al*., 2014]. They demonstrate a clustered and patchy distribution. They consist of two to four layers, with the two outermost layers consisting of isopachous 1 mm thick cement layers that are usually more resistant than the middle layer(s) and suggesting that they formed in the phreatic zone or water-saturated environment possibly before complete lithification of the mudstone [*Siebach et al*., 2014]. In some cases, they appear to substitute laterally for nodules and hollow nodules interpreted as early diagenetic concretions [*Grotzinger et al*., 2014; *Stack et al*., 2014]. Plateau-like features are interpreted to be exhumed subhorizontal crack fills [*Siebach et al*., 2014]. The raised ridges are overwhelmingly restricted to the Sheepbed member [*Grotzinger et al*., 2014; *McLennan et al*., 2014] (Figure 1), though at least one raised ridge may extend into the basal bed of the Gillespie member, which directly overlies the Sheepbed member [*Siebach et al*., 2014]. The Sheepbed mudstone is interpreted to be an exhumed and exposed lakebed at the distal end of an alluvial fan [*Grotzinger et al*., 2014]. Further details on the physical sedimentology, structure, and distribution of these features are reported in *Grotzinger et al*. [2014] and [*Siebach et al*., 2014].

2. Analytical Methods

2.1. The ChemCam LIBS Instrument

In LIBS, a high-intensity laser pulse is used to ablate a small amount of material from a target thereby creating a plasma at the surface of the target. The spectrum of the plasma, formed from the atomic emission lines of all elements present, is recorded and can be later processed for quantitative elemental analyses. By using multiple laser shots at a given location, the laser can effectively be used to remove dust on the surface or drill down into a sample and generate plasmas at increasing depths with each successive shot. Therefore, the LIBS

technique is particularly well suited for investigating surface coatings on solid materials and performing chemical depth profiles [e.g., *Vadillo and Laserna*, 1997; *St-Onge and Sabsabi*, 2000; *Lanza et al*., 2012, 2014a]. The rate of penetration, i.e., the amount of ablated material, with each laser shot is dependent on both laser (e.g., power, beam diameter, and pulse rate) and target (e.g., density, hardness, and cohesiveness) characteristics. While LIBS has been used for investigating layers and performing depth profiles in numerous industrial and pharmaceutical applications, as well as with painted artwork [*Vadillo and Laserna*, 1997; *St-Onge and Sabsabi*, 2000; *Madamba et al*., 2007; *Kim et al*., 2007], its use in investigating complex, geological coatings or multilayered mineral deposits has been limited [cf. *Cousin*, 2012; *Lanza et al*., 2012; *Meslin et al*., 2013 (C. Lefebvre, et al., Depth-resolved chemical mapping of rock coatings using Laser-Induced Breakdown Spectroscopy: Implications for geochemical investigations on Mars, submitted to *Planetary and Space Science*, 2014)].

The ChemCam instrument on the Curiosity rover uses a mast-mounted laser and telescope optical detector head as well as a combination of three body-mounted spectrometers [*Maurice et al*., 2012; *Wiens et al*., 2012]. The Q-switched pulse Nd:KGW laser emits a 1067 nm laser and can operate at 3 Hz with a pulse duration ≤5 ns [*Maurice et al*., 2012]. The three spectrometers cover a nearly continuous spectral range of 240–850 nm over 6144 channels with a variable spectral resolution of 0.15 nm (UV range) to 0.61 nm (visible and near-infrared range) [*Wiens et al*., 2012]. ChemCam LIBS analyses typically involve 30 or 50 laser shots at each point in a raster of several points, including lines of 5, 10, or 20 points or in two-dimensional arrays of 3×3 or 5×5 points. Multiple laser shots help to minimize fluctuations in laser power, while rasters help to assess heterogeneities in sample composition and provide improved compositional sampling. In addition, more extensive depth profiles (up to 600 shots/point) are performed selectively. Generally, spectra from every laser shot are downlinked to Earth (though onboard averaging is possible). The laser spot size ranges from 350 to 550 μm depending on the distance to target.

2.2. The ChemCam Remote Microscopic Imager

ChemCam also includes a panchromatic black and white, high-resolution telescopic imager: the Remote Microscopic Imager [*Maurice et al*., 2012; *Le Mouélic et al*., 2014]. The RMI's circular field of view is 20 mrad in diameter for 1024×1024 pixels with a resolution of approximately 40 μrad [*Le Mouélic et al*., 2014; *Langevin et al*., 2013]. This provides a spatial resolution of approximately 120 μm at a distance to target of 3 m. The RMI is critical to assessing the exact location of laser shots on targets and to place the analytical results in proper context [cf. *Meslin et al*., 2013]. The images also provide some indication of the nature of the target (i.e., rock hardness and dust thickness). Typically, pre- and post-LIBS RMIs are collected, and occasionally, additional RMIs are also collected along rasters in order to provide full coverage of all analysis locations. The details of the RMI image processing are described in *Le Mouélic et al*. [2014].

2.3. Data Processing

Each experiment involves recording a dark spectrum before and after each LIBS analysis. A dark spectrum is identical to a LIBS spectrum except the laser is not fired. Data processing of the LIBS spectra involves several steps including subtracting the background light signal, removing the LIBS produced electron continuum, calibrating for the wavelength, applying a wavelength-dependent correction for the instrument response, and normalizing to the total signal intensity in order to minimize effects of fluctuations in laser power [*Wiens et al*., 2013]. Individual LIBS spectral lines are identified using a dedicated database of spectra collected under Mars ambient conditions [*Cousin et al*., 2011].

Quantitative major oxide weight percentages are estimated using a partial least squares (PLS) model developed by the ChemCam team and which uses a training set of laboratory samples analyzed under Mars ambient conditions. The PLS algorithm determines the principal components of the large number of training set spectra and uses these to fit the unknown spectrum to provide a quantitative elemental composition [e.g., *Clegg et al*., 2009]. The training set and resulting PLS model are both fully described in *Wiens et al*. [2013], and the training set spectra are available in NASA's Planetary Data System. The specific model used a so-called PLS2 algorithm which regresses all elements simultaneously. The ChemCam team has since migrated to a PLS1 algorithm in which individual elements are regressed separately. This allows customization of a few parameters such as the way the spectra are normalized and the number of principal components used in the fit. The customization for each major element

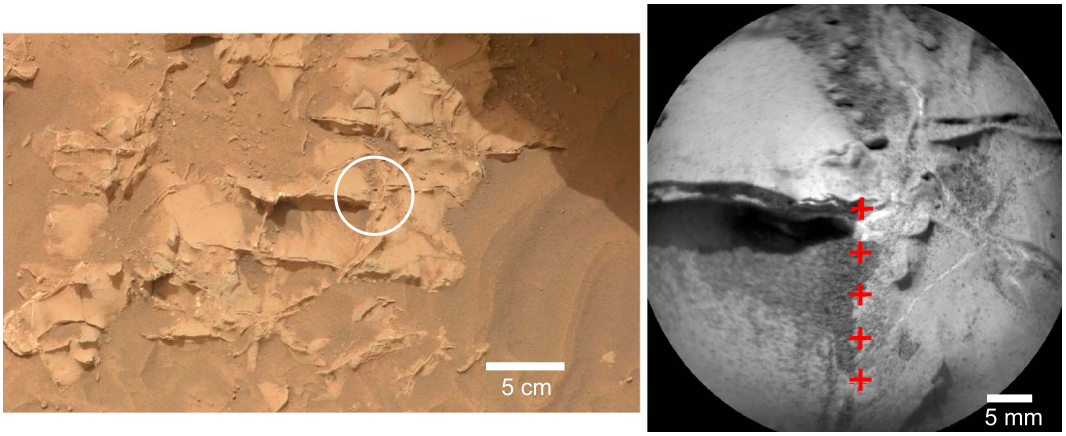

Figure 2. (left) Mastcam M100 2 × 1 mosaic of raised ridges at Rowatt in Yellowknife Bay. The circle denotes the field of view of the corresponding ChemCam RMI image. (right) The 1 × 5 raster of analysis locations (sol 133) taken from a distance of 2.8 m from target to mast unit are highlighted by the red crosses. Here the laser has displaced dust at the surface of the target. Only one of the five locations is on the raised ridge. At this distance, the laser spot size is approximately 400 μm.

resulted in relatively significant improvements to the model. The root-mean-square error product (RMSEP) of the model gives a good estimate of the absolute accuracy, with the following values for SiO_2, TiO_2, Al_2O_3, FeO_T, MgO, CaO, Na_2O, and K_2O: 7.1, 0.55, 3.7, 4.0, 3.0, 3.3, 0.7, and 0.9. The absolute errors near the center of the distribution are generally lower than this so that these RMSEP values are generally conservative for the error when quoting an absolute abundance. Quantification is either done on average spectra for each point in a raster or on the single-shot spectrum for each analysis. Lithium abundances were estimated using a univariate model as described in *Ollila et al*. [2014].

In general, when comparing two different compositions, the analytical precision rather than absolute accuracy is the applicable parameter. For example, results from the Alpha Particle X-ray Spectrometer (APXS) instrument are generally reported with only the precision and not the accuracy. An upper limit on the precision of ChemCam measurements can be determined from the standard deviations of a large number of observations of the different groups of similar, fine-grained targets at Yellowknife Bay (N. Mangold, et al., Chemical variations in Yellowknife Bay formation sedimentary rocks analyzed by ChemCam onboard the Curiosity rover on Mars, submitted to *Journal of Geophysical Researh: Planets*, 2014). These data show standard deviations in the range of ±1.0–2.0 wt % for SiO2 and ±0.1–0.9 wt % for the other major element oxides. All of these standard deviations are far smaller than the absolute errors given by the RMSEP. Here we use the standard deviation of 33 measurements on the Sheepbed mudstone (drilled target and brushed locations, with all analyses of diagenetic features removed), as an estimate of the analytical precision and use this in comparing the raised ridges to the Sheepbed host rock. These standard deviations are upper limits on the actual precision as they include target effects from grains of heterogeneous compositions as well as the natural variability in target composition. Another measure of the precision is obtained by comparing an ensemble of similar observations of ChemCam's onboard calibration targets [*Fabre et al*., 2011, 2014; *Vaniman et al*., 2012]. Such a comparison of analyses performed in the Rocknest location yields similar precision estimates to those mentioned above [*Blaney et al*., 2014].

2.4. Observations of Raised Ridges in the Sheepbed Mudstone

Multilayered, fracture-filling resistant raised ridges were first observed and imaged at Discovery Creek and Rowatt on sols 125 and 133 (a sol is a Martian solar day and the numbering used begins with the start of the Mars Science Laboratory (MSL) landed mission), respectively (Figure 2) [*Siebach et al*., 2014, supplementary figure] as the Curiosity rover entered a low-lying region known as Yellowknife Bay [*Grotzinger et al*., 2014]. More detailed and systematic ChemCam LIBS observations were made on John Klein (sols 155 and 165), McGrath (sols 185, 189, 193, and 226; Figure 1), and Lady Nye (sol 290). Detailed LIBS depth profiles were performed on McGrath (sol 234; 5 points of 150 laser shots each) and Lady Nye (sols 285 and 288; 3 points of 600 laser shots each; see below). The details of these analyses are summarized in Table 1.

Table 1. Summary of ChemCam LIBS Observations on Raised Ridges at Yellowknife Bay, Gale Crater

Sol	Target Name	Distance (m)	Raster Type	Laser Shots/Location	Notes
125	Discovery Creek	5.8	3 × 3	30	Poor signal due to distance to target; results not quantified
133	Rowatt	2.8	5 × 1	30	Only location 5 is on raised ridge.
155	John Klein	5.4	1 × 5	30	All five locations on raised ridge
165	John Klein RP2	3.0	3 × 3	30	All locations missed raised ridge.
165	John Klein RP3	3.0	3 × 3	50	Locations 1–3 and 7 not on raised ridge
185	McGrath 1	2.3	1 × 10	30	Locations 1 and 7–10 not on raised ridge
189	McGrath 2	2.3	10 × 1	30	Only locations 1–4 on raised ridge
193	McGrath 3	2.3	10 × 1	30	All locations missed raised ridge.
226	McGrath 4	2.3	1 × 20	30	Locations 18–20 not on raised ridge
234	McGrath 5	2.3	1 × 5	150	Depth profiles
285	Lady Nye 1	2.5	1	4 × 150	Depth profile
286	Lady Nye 2	2.5	1	4 × 150	Depth profile
288	Lady Nye 3	2.5	1	4 × 150	Depth profile
290	Lady Nye 4	2.4	15 × 1	30	Locations 8–11 in dust

In LIBS, the ablation rate is highly dependent on the laser and on the material properties. Preflight tests with the ChemCam engineering qualification model and flight model gave estimated depth profiling rates of 0.3–0.85 μm/shot for basalt and 0.55–0.8 μm/shot for calcite, both at a distance of 3 m in 9.3 mbar of air [*Wiens et al.*, 2012]. Lefebvre et al. (submitted manuscript) reported much higher ablation rates of 4–6 μm/shot for carbonate-rich coatings on basalt, analyzed in a CO_2 atmosphere at Martian atmospheric pressure (6.6 mbar). However, in these experiments the laser system was different from that in ChemCam (1 Hz, 8 ns, and 16 mJ). On Mars, the lower temperatures will provide a higher laser power (the ChemCam laser operates optimally around −10°C rather than at room temperature), and the lower pressure and lower gravity may favor removal of ablated material [cf. *Vadillo and Laserna*, 1997; *Novotny et al.*, 2007]; together, these factors are expected to lead to greater ablation rates on Mars [*Cousin*, 2012]. For these analyses, we estimate an average ablation rate of 1.0–5.0 μm/shot. This would represent a total penetration of 150–750 μm for McGrath 5 and 600–3000 μm for the Lady Nye 600-shot depth profiles. As expected, the overall total intensity decreases with depth for each of the depth profiles. This is expected as the plasma becomes increasingly confined in the crater as it gets deeper with each successive shot (Figure 10). Normalization to total intensity is part of the normal data processing [*Wiens et al.*, 2013], and the PLS results therefore take this effect into account.

3. Results

3.1. Near-Surface Analyses

The ChemCam LIBS compositional averages for the raised ridges are summarized in Table 2 for a total of 65 points on three main targets: John Klein, McGrath, and Lady Nye (see Table S1 in the supporting information). In addition, a single location on Rowatt (Figure 2) and two locations on John Klein RP2 were also analyzed but are not discussed herein in order to simplify the discussion. For Discovery Creek

Table 2. Average Compositions of Targets With Multiple Analyses of Raised Ridges in the Yellowknife Bay Area[a]

Target	SiO_2	TiO_2	Al_2O_3	FeO_T	MgO	CaO	Na_2O	K_2O	Total
John Klein ($n = 10$)	49.6	0.9	6.8	17.6	11.4	4.8	2.3	0.4	93.9
SD	5.7	0.3	2.0	2.1	4.3	1.4	0.6	0.4	
McGrath ($n = 31$)	42.5	0.9	6.1	17.4	8.3	5.3	2.0	0.2	82.6
SD	2.1	0.2	1.3	1.0	1.8	1.1	0.2	0.2	
Lady Nye ($n = 24$)	46.1	0.8	6.9	16.4	8.4	6.6	2.0	0.2	87.5
SD	4.2	0.2	0.8	0.9	1.3	0.8	0.3	0.2	
Sheepbed mudstone	46.1	1.1	8.1	16.4	5.7	6.6	2.4	0.7	87.2
SD	1.9	0.2	0.6	0.8	0.4	0.9	0.2	0.2	

[a]Only data for locations on actual ridges (as determined by RMI mosaics) are reported. The standard deviation is provided for each group of analyses. The average composition of the Sheepbed member (drilled targets and brushed locations; diagenetic features excluded), determined from 33 ChemCam analyses (Mangold et al., submitted manuscript), is also reported. Note: for the Lady Nye depth profiles, we include each 150 shot series as a single analysis for averaging. SD = standard deviation.

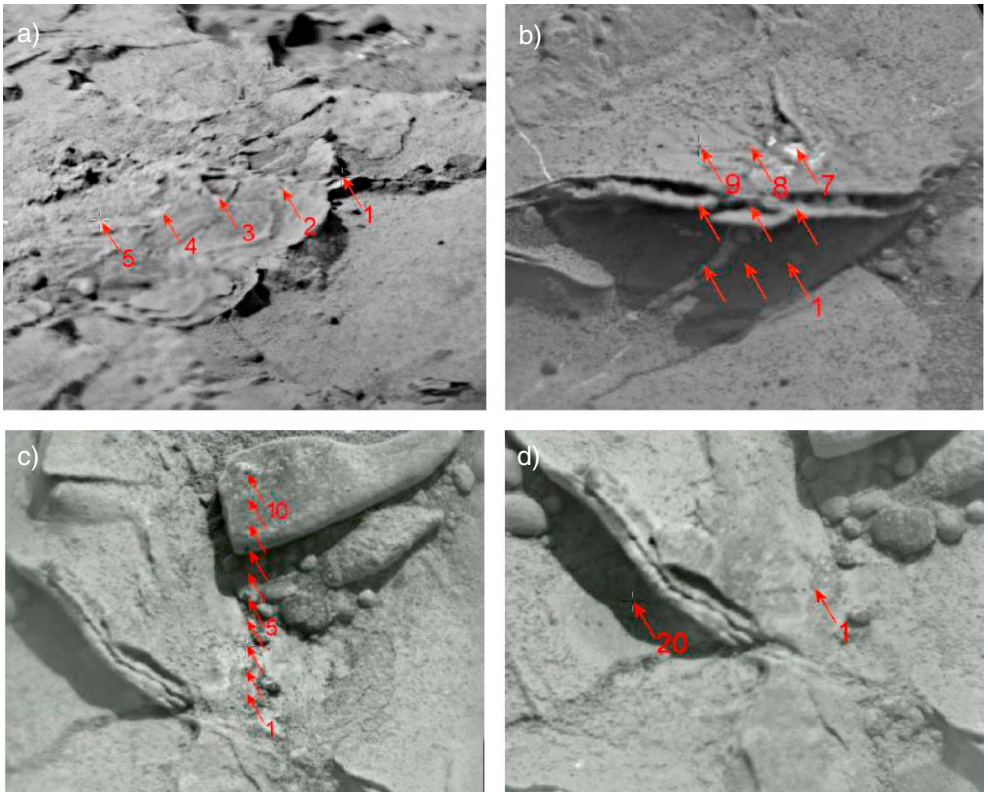

Figure 3. RMI mosaics of selected raised ridges targeted by ChemCam. (a) John Klein, 1 × 5 (sol 155); (b) John Klein RP3, 3 × 3 (sol 165); (c) McGrath 2, 1 × 10 (sol 189); (d) McGrath 4, 1 × 20 (sol 226).

the elevated distance (5.4 m) to the target produced spectra with a poor signal-to-noise ratio, and laser spot locations cannot be seen clearly on the post-LIBS RMI; the data were not quantified. Close inspection of RMI images enabled us to determine if individual locations in a raster were on a raised ridge or not (Figures 2–5). Only those that appear to hit the raised ridges are reported in Table 2. Overall, the raised ridges are most significantly enriched in MgO by a factor of 1.2–1.7 compared to the Sheepbed member in which they occur (Figure 6). In addition, both the quantitative PLS data (Figure 7) and single line peak intensity data (Figure 8) show that there is an anticorrelation between MgO and Al_2O_3, especially strong for the McGrath target. At the scale of the ChemCam analyses, there does not appear to be a correlation between MgO and FeO or between MgO and SiO_2. The average FeO_T content of the raised ridges is 16.4–17.6, which is similar to the average composition of the Sheepbed mudstone (Mangold et al., submitted manuscript) (Figure 6). Average TiO_2 values are slightly lower in the raised ridges compared to the Sheepbed member, while K_2O values are even more depleted in the raised ridges (Table 2 and Figure 6). We describe below each individual analysis and provide the ChemCam sequence identification number in the format ccamXXXXX.

For John Klein (sol 155, 1 × 5 diagonal, 30 shots, ccam01155, 5.4 m), the raster appears to start on a protruding raised ridge and then goes across a flat, subhorizontal oriented part of the ridge (Figure 3a). This is likely a plateau-like, subhorizontal, exhumed and exposed part of a resistant crack filling as described by *Siebach et al.* [2014]. All the locations except for location 1 show elevated MgO. In fact, the average MgO content of location 3 shows the highest average (17.0%) of all the raised ridge analyses (with a single-shot maximum of 17.7%). The SiO_2 concentration is higher by approximately 10 oxide wt % compared to the other targets, the standard deviation is higher, and the total for the analyses averages 104 wt %.

For John Klein RP3 (sol 165, 3 × 3, 50 shots, ccam03165, 2.98 m), locations 1–3 are likely on the background rock, while locations 4–9 are on subhorizontal oriented ridges (Figure 3b). Locations 4–6 have the highest average MgO values (11.2–15.6%; with a single-shot maximum of 16.2% in location 5) of the raster, which is

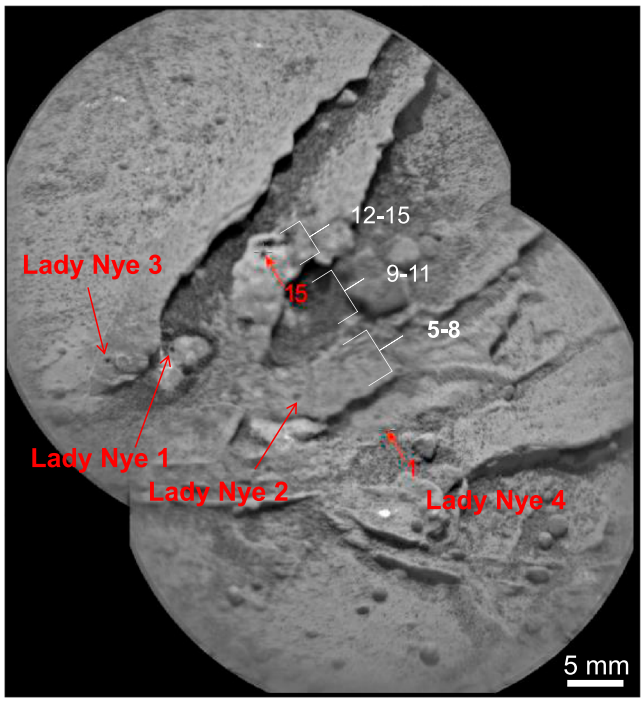

Figure 4. RMI mosaic of Lady Nye target showing the locations of three depth profiles (Lady Nye 1 to 3) and 1 × 15 raster (Lady Nye_4). There is an abundance of dust covering the target in some cases (e.g., locations 9–11 in Lady Nye_4). In Lady Nye_1, the laser shots have clearly moved dust and exposed the underlying material. Locations 12–15 of the raster correspond to the layer analyzed in Lady Nye_1, and this layer is most enriched in MgO. Locations 5–8 correspond to the layer analyzed in Lady Nye_2.

consistent with other analysis locations on more resistant, outermost cement layers. Location 7 has the lowest oxide total (75.4%) and highest CaO (14.2%) and corresponds to a bright white area observable in the RMI where there are clearly white veins cutting across the raised ridge (Figure 3b). The spectrum for this location also shows S lines, and this is consistent with observations of Ca-S-rich veins throughout the Yellowknife Bay region [*Nachon et al.*, 2014].

The McGrath target was analyzed on multiple sols using various rasters, including a series of five 150-shot depth profiles. We use the term "McGrath" to refer to the overall target rock and specify the actual analysis (e.g., McGrath 1) when referring to individual analyses. In McGrath 1 (sol 185, 1 × 10, 30 shots, ccam07184, 2.3 m), locations 1–6 appear to be on a raised ridge, but only locations 2, 5, and 6 show an elevated MgO (7.2–9.4%). Location 1 is particularly low in MgO, but it also appears to be very dusty in the RMI image (not shown). Locations 2–6 appear to be outermost cement layers. Locations 7–10 are not on raised ridges but instead on pebbles and dust. For McGrath 2 (sol 189, 10 × 1, 30, ccam01189, 2.3 m) locations 1–4 are on the outermost cement layer of the ridge (Figure 3c), and these show a MgO content of 8.9–9.9 wt %. Locations 5–10 are on pebbles or dust. In McGrath 3 (sol 193, 10 × 1, 30 shots, ccam01193, 2.3 m), location 1 may be on the edge of the ridge middle layer. Locations

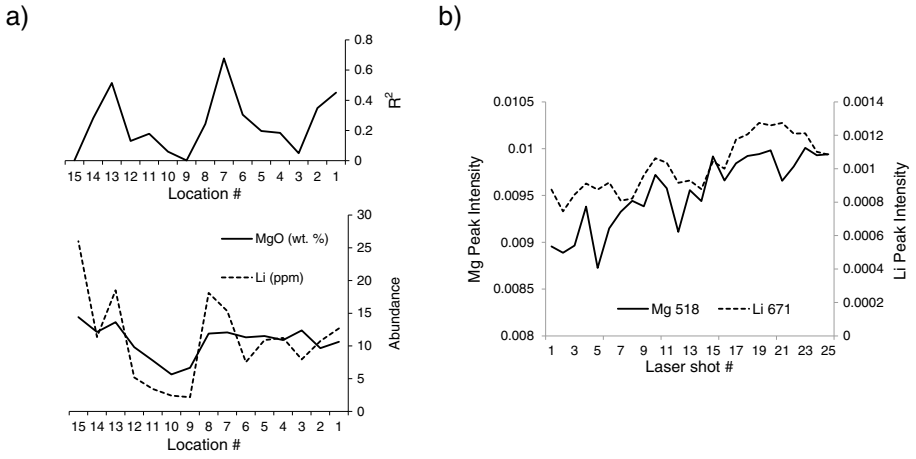

Figure 5. Lady Nye_4 raster (sol 290, 1 × 15, 30 shots, ccam01290) across raised ridge. (a) The average MgO (wt %) and Li (ppm) concentrations are plotted for each location (bottom). There is a general correspondence between high MgO and high Li. The R^2 values for each spot for shots 6–30 (first five shots removed) (top). However, the locations with low MgO and Li (8–11) appear to be in an area with a thick dust cover. (b) For location 7, shots 6–30 (first five shots removed) show the strongest correlation ($R^2 = 0.68$) between MgO and Li abundance.

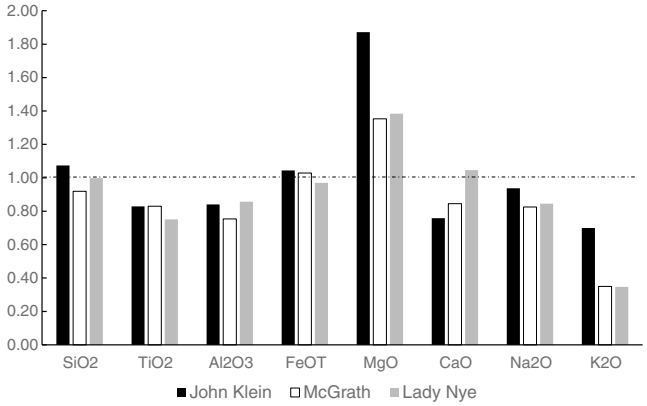

Figure 6. Comparison of the average composition of raised ridges to the Sheepbed member. The average composition of three raised ridge targets is normalized to the average composition of the Sheepbed member of Yellowknife Bay. See Table 2 for data. The raised ridges are consistently enriched in MgO but slightly depleted in TiO_2, Al_2O_3, and K_2O when compared to Sheepbed. Sheepbed ChemCam data are from Mangold et al. (submitted manuscript).

2–5 are on the outermost cement layer. Locations 6–10 are not on the raised ridge. In the McGrath 4 raster (sol 226, 20 × 1, ccam01226, 2.3 m), several locations were on the raised ridge (Figure 3d). In fact, the data suggest that ChemCam successfully targeted both outer layers of resistant cement coating the fracture walls, as well as an inner, less resistant cement layer. The outermost layers are consistently more enriched in MgO than the central layer as first observed by *McLennan et al.* [2014]. In this case, the more MgO-rich layers also show elevated Li, and MgO is strongly anticorrelated with Al_2O_3 (Figure 7).

The Lady Nye_4 raster (sol 290, 1 × 15, 30, ccam01290, 2.43 m) targeted a horizontal profile across the raised ridge layers. However, not all of the LIBS craters are clearly visible in the RMIs, partly due to variable dust cover of the target (Figure 4). In particular, locations 8–11 are in dust, and these show the lowest MgO and highest Al_2O_3 abundances. Locations 13–15 are in a distinct resistant cement layer, and these locations show the highest MgO abundance, with location 15 showing the highest average (of the 30 shots) at 9.7%. This resistant cement layer corresponds to the cement layer analyzed in the Lady Nye_1 depth profile (see below). The upper part of the depth profile (first 70 shots) does show an average MgO abundance that is consistent with that in locations 13–15 of the raster. However, the MgO abundance increases to greater than 10% for most of the rest of the 600 shots (see below). Although difficult to say with confidence, locations 4–8 may be in a distinct less resistant cement layer and these show moderately high MgO (average 6.8–7.7%). This layer corresponds to the layer analyzed in the Lady Nye_2 depth profile, which indeed shows a lower MgO abundance throughout the depth profile (average of 9.1%). Like for McGrath, there is a moderate correlation of MgO and Li in the locations with the highest MgO in Lady Nye (R^2 as high as 0.7; Figure 5).

3.2. Depth Profiles

We successfully performed a series of five 150-shot depth profiles (Sol 234, 1 × 5, 150 shots, ccam02234, 2.3 m) across the McGrath 5 target (Figure 9). The first three locations are in the outermost layer and show, on

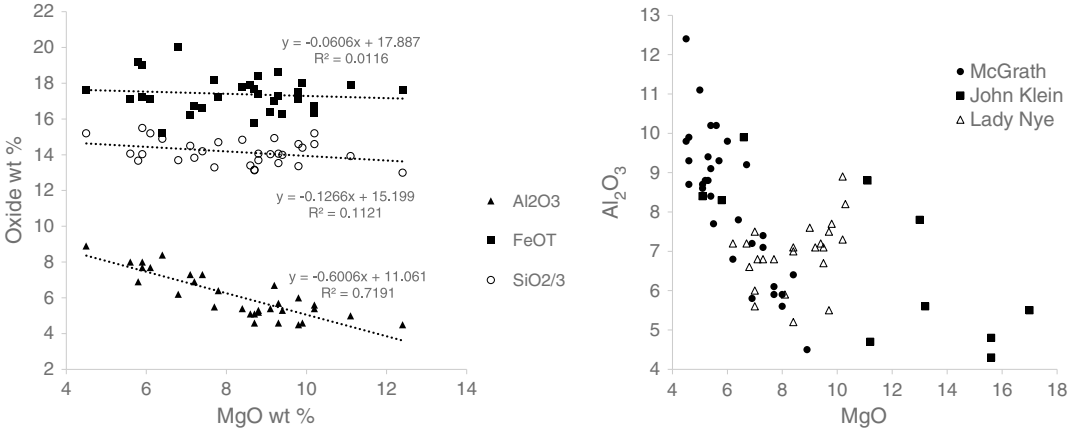

Figure 7. (left) Concentration of MgO compared to SiO_2, FeO_T, and Al_2O_3 for the McGrath target. There is a strong correlation between MgO and Al_2O_3 but no obvious correlation between MgO and SiO_2 or between MgO and FeO_T. (right) Plot of Al_2O_3 and MgO for the three main targets showing a general anticorrelation, especially strong for McGrath ($R^2 = 0.72$).

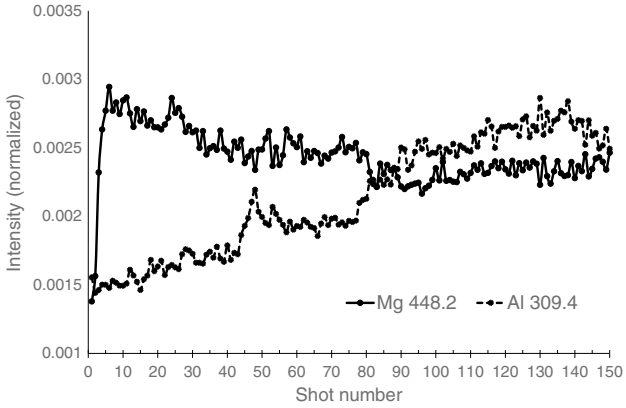

Figure 8. Normalized peak intensities for the Mg (448.2 nm) and Al (309.4 nm) lines for the first 150 shots of the ChemCam depth profile on Lady Nye 2 (sol 286, 2.5 m, 600 shots, ccam01286).

average, the highest MgO (Figure 9), and lowest Al_2O_3, which is consistent with the comparable analyses in the McGrath 4 1 × 20 line raster. Locations 4 and 5 are on the middle, less resistant layer and show lower MgO, but higher Al_2O_3, again confirming the analysis of this middle layer in the McGrath 4 raster. There are definite changes with depth in all five profiles, and these may reflect a layered structure to the raised ridges. Locations 1 to 3 show a general decrease in MgO over the 45 shots, with some variation, followed by a general increase for the remainder of the 150 shots. For location 3, the initial part of the depth profile shows a slightly lower MgO than locations 1 and 2 but then increases rapidly to match the two other profiles. This could reflect a thinner upper layer that is intermediate between the layer at locations 1 and 2 and what is at locations 4 and 5. The profiles at spots 4 and 5 are both offset to lower MgO values compared to the three other profiles. However, after about 50–60 shots, they both show an increase in MgO, though not reaching the levels of the higher profiles. This may reflect the fact that the laser initially was hitting a low-MgO layer, which is consistent with the inner layer seen in the line raster. As the laser "drilled" in the target, it may have passed into the MgO-rich layer which would be below (to the left of point 5 in the RMI image in Figure 9). As such, these depth profiles may represent the third dimension of the multilayered structure of the raised ridges.

For Lady Nye, three 600-shot depth profiles were performed in addition to the 1 × 15 line raster. In all three depth profiles, variations can be seen with depth for the major oxides though the most significant changes with depth occur in the first 150 shots. Lady Nye_1 (sol 285, 1 × 1, 600 shots, ccam06284, 2.5 m) shows an initial MgO content of approximately 8 wt % but then increases to 10% over the course of the first 150 shots (Figure 10). This layer would be on top of the Lady Nye_2 layer; the Lady Nye_3 layer is not analyzed in this profile. For Lady Nye_2 (sol 288, 1 × 4 × 150, ccam 01286, 2.5 m), the exact stratigraphic position of this layer is not clear, but it also shows an increase in MgO, from 8.4% to 9.7%. The Lady Nye_3 (Sol 288, 1 × 4 × 150, ccam 02286, 2.5 m) location appears to be on a layer that overlaps the other two layers. Overall, there is little change with depth and the average MgO is 9.6%. The Lady Nye target appears to be a more complex target and does not clearly show the three-layer structure as does McGrath. Nevertheless, all the depth profiles show variations with depth. However, the differences in MgO content in Lady Nye appear to be smaller than in McGrath.

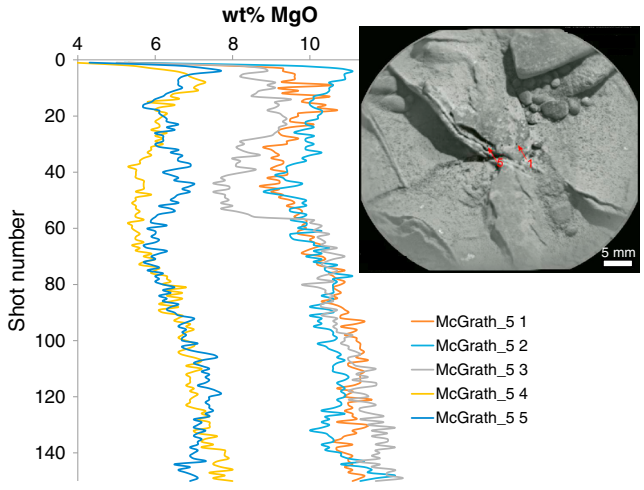

Figure 9. MgO content in McGrath 5 depth profiles (sol 234, 1 × 5, 150 shots, CCAM 02234). The RMI (inset) shows that spots 1 to 3 are on the MgO-rich outer layer, while spots 4 and 5 are on the MgO-poor middle layer, as seen in the McGrath_4 1 × 20 line raster. Variations in MgO content with depth can be explained by the laser ablating through different layers of varying composition.

The depth profiles are characterized by gradual changes in composition with depth; in some cases these changes are quite subtle. This can be explained in part by natural variations in composition and heterogeneities in the targets themselves. However, terrestrial LIBS studies on natural rock coatings and multilayered mineral deposits are also informative. Lefebvre et al.

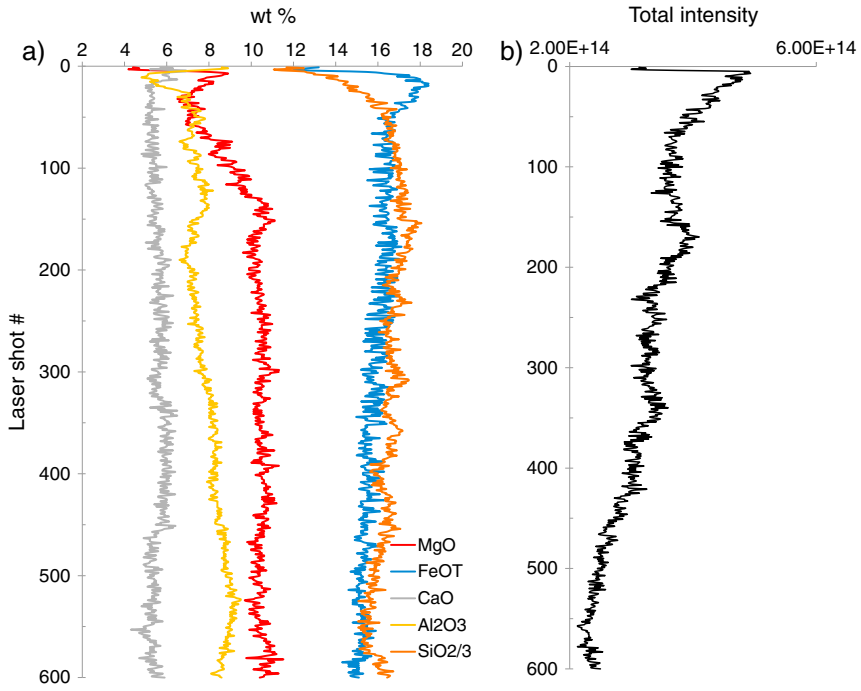

Figure 10. Six hundred-shot depth profile for Lady Nye_1 (sol 285, single spot, 600 shots, ccam06284) showing (a) major oxide concentration as a function of shot number and (b) total intensity as a function of shot number. The most significant variations in composition occur in the first 150 shots, especially for MgO, SiO_2, and FeO. The total intensity decreases with depth as the plasma becomes confined in the crater created by the laser.

(submitted manuscript) noted that for multilayer mineral coatings on rocks, the transition between different layers and between coatings and the rock underneath for a single element was not abrupt but rather gradual. *Lanza et al.* [2012, 2014b] also noted this characteristic LIBS coating signature. These trends with depth in the LIBS data can be explained by a combination of natural sample heterogeneities but also the physical interaction of the laser with the target. Briefly, the laser power has a Gaussian distribution [*Maurice et al.*, 2012]. Therefore, the central most part of the laser will potentially ablate more rapidly than the periphery, though more detailed work on geological materials is required to better understand this behavior. In addition, the plasma itself may interact with the walls of the crater as it expands. Thus, the depth profile may, in fact, be combining the ablated material from the crater and the integrated analysis of the crater walls by laser and plasma interaction. Loose particles may also be displaced and redeposited though we do not have direct evidence of this. Continuing laboratory studies of LIBS depth profiles and laser-plasma-sample interactions in natural geological materials will greatly help to interpret these unique chemical data sets from ChemCam.

4. Discussion

4.1. Summary of Raised Ridge Chemistry From ChemCam Analyses

Systematic analyses by ChemCam of the raised ridges in the Sheepbed mudstone reveal that the ridges have a distinct composition as compared to the host mudstone. Specifically, the raised ridges show a consistent, though variable, enrichment in MgO when compared to the Sheepbed mudstone, whereas TiO_2 and Al_2O_3 are slightly depleted and K_2O is significantly depleted (Figure 6). MgO in the raised ridges is also strongly anticorrelated with Al_2O_3 (Figures 7 and 8), though not with SiO_2, which shows no correlation with MgO. This suggests that the raised ridges contain a Mg-rich and Al-poor, Si-bearing phase with a similar SiO_2 content as the host rock. The elevated MgO and presence of SiO_2 cannot be attributed simply to an increased abundance of forsterite, enstatite, or other primary igneous Mg-rich silicate as the MgO/SiO_2 is incompatible with such phases, and it is unlikely that the ridges contain much if any detrital material [*Siebach et al.*, 2014]; the isopachous geometry of the raised ridge cements strongly suggests precipitation of minerals in the

phreatic groundwater zone. Similarly, the compositions observed cannot be attributed uniquely to carbonates, sulfates, or chlorides. Some amount of CaO is likely attributed to the presence of Ca sulfate, present as thin veins observed in some RMI mosaics, and as reported in *Nachon et al.* [2014]. Some amount of S (as well as possibly Cl, Mn, and other minor/trace elements), not quantified here, can also account for oxide analysis totals being less than 100%. If a nonsilicate Mg-rich phase was present in abundance (more than a few weight percent), we would expect an anticorrelation between MgO and SiO_2. In addition, we would also expect an anticorrelation between MgO and the total of the analysis of the oxides, as is seen with CaO for Ca sulfate veins analyzed by ChemCam at Yellowknife Bay [*Nachon et al.*, 2014]. None of these observations are seen for the analyses here. Therefore, it is unlikely that abundant Mg carbonates, Mg sulfates, or Mg chlorides are present in the raised ridges, at least not in abundance of more than a few weight percent.

Based on the McGrath target, and to a lesser extent on the Lady Nye target, the raised ridges also appear to consist of multiple layers with different compositions (Figure 12). This variation in composition of the different layers can be considered as a cement stratigraphy [cf. *Kauffman et al.*, 1988; *Yamin Ali*, 1995; *Wolela and Gierlowski-Jordesch*, 2007]. We interpret the variations with depth as representative of changes in fluid composition over time, or distinct phases of cement precipitation, as the walls of the fractures were filled isopachously by the different episodes of mineral precipitation. Although we have no constraints on the time interval represented by these fracture-filling veins, we do know that they were formed after cracking of the, at least, partly lithified sediment and before the later stage of fracturing and infilling by Ca sulfate. The cracks and their isopachous fills are regarded as an early diagenetic phenomenon since they show lateral substitution with concretions (nodules and hollow nodules) [*Stack et al.*, 2014]. Further details on the possible mode of formation are provided below.

4.2. Comparison With APXS, CheMin, and Sample Analysis at Mars Results

A similar enrichment in MgO and anticorrelation between MgO and Al_2O_3 were also observed in the Alpha Particle X-ray Spectrometer (APXS) data for the McGrath target [*McLennan et al.*, 2014]. As first noted in *McLennan et al.* [2014], the McGrath raised ridges also show a correlation between MgO and Li based on ChemCam data. As shown in Figure 5, the Lady Nye target also generally shows this enrichment of Li in the most Mg-rich points. Clay minerals, in particular trioctahedral Mg-rich smectites, can be effective at trapping Li, either adsorbed on their surface or within the crystal structure, most commonly substituting for Mg^{2+} in octahedral sites, though presumably in interlayer space as well [*Starkey*, 1982; *Decarreau et al.*, 2012]. Li-bearing smectites have also been described from fluviolacustrine settings [*Starkey*, 1982, and references therein]. *McLennan et al.* [2014] also reported elevated Fe and Mg, together both correlated with Cl, and interpreted these as reflecting the presence of an assemblage of Mg-Fe-Cl-bearing phases. Based on mass balance calculations, *McLennan et al.* [2014] estimated a composition (by weight) of $SiO_2 = 45\%$, $FeO_T = 35\%$, MgO = 18%, Cl = 3%, >1300 ppm Ni and Br (each) for the raised ridges and proposed a possible mixture of Mg-rich, Al-deficient smectitic clays and Cl-bearing Fe oxides, such as akageneite, in part because some akaganeite was also detected by the CheMin instrument in the two drilled samples at Yellowknife Bay [*Vaniman et al.*, 2014]. Based on the ChemCam data presented here, the FeO_T appears to be lower than 35% (maximum value of 20%). In addition, at the scale of ChemCam analyses, there is no obvious correlation between MgO and FeO_T as noted by *McLennan et al.* [2014] based on APXS data, likely because the APXS instrument integrates over a much larger area (roughly a circle with a diameter of 1.5–2.0 cm). ChemCam was not able to detect Cl in these targets, likely because of its low concentrations (i.e., 1–2 wt %, as per APXS measurements) [*McLennan et al.*, 2014]. Some of the Cl found to be enriched in the raised ridges may also be related to coprecipitated evaporitic chlorides, including NaCl as the ridges also contain 2 wt % Na_2O [*McLennan et al.*, 2014].

X-ray diffraction analysis by the CheMin instrument of the drilled rocks Cumberland and John Klein, both in the Sheepbed member and located within 2–3 m of the John Klein and McGrath ChemCam targets, revealed abundant smectitic clays including possibly an Fe-bearing saponite, as well as magnetite and minor amounts of akaganeite [*Vaniman et al.*, 2014]. Evolved gas analyses with the Sample Analysis at Mars (SAM) instrument also indicate the presence of clay minerals based on the evolution of water at approximately 800°C, which is consistent with dehydroxylation of a smectitic clay mineral [*Ming et al.*, 2014]. Unfortunately, the raised ridges were not drilled, and consequently, no CheMin or SAM observations were made of them directly. However,

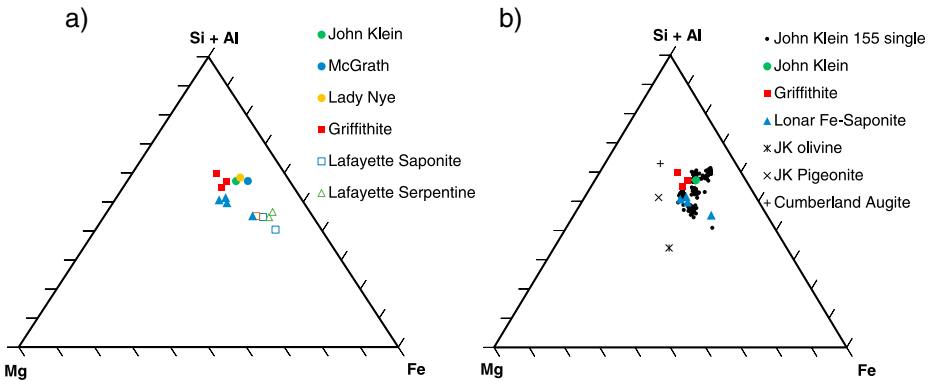

Figure 11. Atomic ratios of the Griffith Park (California) variety of saponite [*Treiman et al.*, 2014]. Fe-saponite from hydrothermally altered Lonar Crater basalts [*Hagerty and Newsom*, 2003] and alteration Fe-Mg phyllosillicates in nahklite meteorites [*Treiman et al.*, 1993; Bridges et al., submitted manuscript] compared to (a) the average composition of the main raised ridge targets and (b) the John Klein target (ccam01155, 1 × 5, 30 shots; first five shots removed), which shows the highest MgO (up to 17.7% MgO). Estimated compositions for Sheepbed olivine, pigeonite, and augite are from [*Vaniman et al.*, 2013] based on CheMin analyses of the John Klein drill sample [after *Changela and Bridges*, 2010].

ifthe cementing material that creates the isopachous linings within the cracks is associated with the same fluid migration event that cemented the mudstone, then it is possible that the CheMin and SAM data are highly relevant.

4.3. Inferred Mineralogy of Raised Ridges

Taken together, these observations are most consistent with the presence of a Mg-rich phyllosilicate. More specifically, the raised ridges match closely the composition of an iron- and Mg-containing saponite (Figure 11), such as ferrian saponites described by *Kodama et al.* [1988], randomly interstratified saponite-vermiculite from the Granby basaltic tuff [*April and Keller*, 1992], and "green saponite" from seafloor hydrothermal alteration [e.g., *Andrews et al.*, 1977]. In particular, the compositions resemble the saponite which has been described in the Martian Lafayette nakhlite meteorite [*Changela and Bridges*, 2010] and that has recently been proposed as the main phyllosilicate phase present in the Sheepbed mudstone at Yellowknife Bay based on the CheMin X-ray diffraction results and terrestrial analogues [*Vaniman et al.*, 2014; *Treiman et al.*, 2014]. The composition of this alteration mineral matches closely the composition of the raised ridges, generally within 1–6 wt % for MgO, FeO_T, Al_2O_3, and SiO_2, and including a couple of percent Na_2O. Note that dehydrated (not dehydroxylated) smectite should contain about 4.5 wt % H_2O equivalent, which may be the case for many clays at the surface of Mars, though there is evidence of some variably hydrated smectites in the Sheepbed mudstone [*Vaniman et al.*, 2014]. APXS data for McGrath [*McLennan et al.*, 2014] suggest that the raised ridges may also contain approximately 3–4 wt % CaO, 2–3 wt % $Na_2O + K_2O + P_2O_5$, and 1–2 wt % Cl. As the elements H, S, P, and Cl are not quantified in low abundances by ChemCam using the PLS method, the sum of these (approximately 11–14%) could well account for the missing components in the analysis (Table 2). For McGrath and Lady Nye this amounts to 12.5–17.4 wt %, which is close to the expected value based on the APXS analyses and the assumed hydration, considering the predicted errors on the PLS results. The calibration of hydrogen in the ChemCam analyses is particularly challenging [cf. *Schröder et al.*, 2014], and no obvious correlation was observed between Mg and H for the raised ridges. Even in measurements of the Sheepbed drill holes, where phyllosilicates are known to be enriched based on CheMin analyses [*Vaniman et al.*, 2014], the hydrogen peaks are not particularly high in ChemCam spectra.

Saponites are a group of trioctahedral smectites that generally have Mg in the octahedral site, though Fe-rich varieties also exist, and a chemical solid solution exists between the saponite and nontronite end-members [*Grauby et al.*, 1994]. Saponites commonly form from hydrothermal alteration as veins and vesicles or from the weathering of mafic rocks, in both seafloor and terrestrial alteration systems, and precipitates from aqueous solutions as crack fillings [e.g., *Andrews*, 1980; *Desprairies et al.*, 1989; *April and Keller*, 1992; *Garvie and Metcalfe*, 1997; *Ehlmann et al.*, 2012; *Treiman et al.*, 2014]. The smectite-chlorite transition through chlorite-

saponite mixed-layered mineral series is also common in diagenetic and low-temperature metamorphic systems [*Beaufort and Meunier*, 1994; *Meunier*, 2005]. Generally, corrensite (ordered mixed-layer chlorite-smectite) has a chemical composition between chlorite and saponite, and Mg ions may be present in exchangeable sites. Abundant chlorite does not appear to be present in the Sheepbed mudstone based on the CheMin X-ray diffraction results [*Vaniman et al*., 2014]. However, in one of the drilled mudstone samples (Cumberland), the persistent larger interlayer spacing may be attributed to incipient chloritization by fixation of Mg-hydroxyl groups, likely at near-surface conditions in the presence of a Mg-rich alkaline fluid [*Vaniman et al*., 2014]. By analogy, we do not expect chlorite to be an abundant phase in the raised ridges and suggest instead that the measured compositions are more representative of a Mg-Fe-saponite phase. The lack of abundant chlorite in either the sediment or the raised ridges may suggest that these materials did not undergo extensive burial diagenesis or were not subjected to temperatures above ~80°C after deposition. Therefore, it seems more likely that the composition is representative of a Mg-Fe-saponite phase, rather than a nontronite or chlorite.

However, as proposed by *McLennan et al*. [2014], it is also possible that the raised ridges consist of a mineral assemblage that includes one or more Mg-rich clay minerals and Fe-oxy/hydroxides or Fe-oxy/chlorides (such as akaganeite). In fact, the compositions of the raised ridges plot closer toward FeO on the Aluminum-Iron-Magnesium (AFM) diagram when compared to many Mg-Fe-saponites (not shown) or toward the Fe apex in the atomic ratio plot in Figure 11. This could reflect a cooccurrence of iron oxides, which are common in Mars dust and rocks [e.g., *Morris et al*., 2000; *Bish et al*., 2013; *Vaniman et al*., 2014]. Iron oxides could also serve as nucleation sites for authigenic formation of Fe-rich smectites, such as nontronite, or perhaps Mg-Fe-saponite in a Mg-rich fluid. The variability in composition of the raised ridges may, in fact, be a result of varying proportions of the minerals in the assemblage. While it is entirely possible that the raised ridges contain an assemblage of secondary phases that are different from those in the drilled Sheepbed mudstone, our findings are consistent with the interpretation that the minerals present in the raised ridges are similar to the alteration minerals in the Sheepbed mudstone. The Sheepbed mudstone likely consists of a mixture of basaltic detrital material and authigenic alteration products such as the proposed Fe-saponite [*Vaniman et al*., 2014; *Ming et al*., 2014; *Treiman et al*., 2014]. The composition of the raised ridges may simply represent an authigenic end-member clay mineral phase that has precipitated from the fluids that have also circulated through and interacted with the Sheepbed rocks and precipitated a similar phase as pore filling cements in the mudstone. One possibility is that the Mg enrichment in the raise ridges may be related to Mg enrichment in interlayer sites of the saponite [*Rampe et al*., 2014]. The possible origin of these raised ridges is discussed further in section 4.4.

4.4. Geochemistry of Fluids and Implications for Past Habitability of Mars

Grotzinger et al. [2014] first reported on the occurrence of raised ridges and interpreted them to have originated as early diagenetic cracks that formed in consolidated or partly lithified fine-grained sediments, which were then filled with one or more generations of cement that lined the margins of the cracks. The raised ridges appear to be contemporaneous with nodules and hollow nodules, but they are crosscut by later-stage Ca sulfate veins, which penetratively cut all of the Yellowknife Bay formation and represent a late-stage alteration event with a distinct fluid composition [*Grotzinger et al*., 2014; *McLennan et al*., 2014; *Vaniman et al*., 2014; *Nachon et al*., 2014; *Siebach et al*., 2014].

No obvious textural differences between the different layers of the raised ridges have been observed, suggesting that they likely formed from the same process. This is also supported by the apparent isopachous growth of the cements [*Grotzinger et al*., 2014; *Siebach et al*., 2014]. In addition, the fractures that contain the raised ridges must have been completely filled by cements as later-stage formation of Ca-S veins would have filled, at least partially, any remaining pore space in the fractures. *Siebach et al*., [2014] and *Grotzinger et al*. [2014] have proposed that the raised ridges formed as authigenic cements precipitating from syndepositional pore fluids within synaeresis, or early subaqueous shrinkage, cracks in the mudstone. These are compared to molar tooth structures, which are a terrestrial example of cement-filled synaeresis cracks. However, unlike on Earth where these features are dominated by calcium carbonate, the raised ridges have a unique phyllosilicate composition, which possibly reflects very different atmospheric and source rock conditions than typically encountered in terrestrial sedimentary systems.

However, *Tosca et al*. [2011] did propose that Proterozoic sedimentary talc nodules from Svalbard formed via dehydration of poorly ordered saponitic or kerolite-like Mg-rich silicates within molar tooth structures. Although the innermost, less resistant cement fill layer of the McGrath raised ridge has a similar composition to the Sheepbed mudstone, the enrichment in Mg, especially in the outer layers, cannot easily be explained by input of detrital material, such as injection of mud. We therefore favor a subaqueous, authigenic formation for all the layers of the raised ridges.

Meteoric waters in basaltic terranes on Earth are typically dominated by Mg-Ca-SiO_2, and Mg is one of the more mobile elements in near-neutral solutions. As such, Mg-rich minerals in fluid-filled fractures, porosity, or void spaces are expected to form. In less oxidizing conditions, or at lower pH, iron will also tend to be more mobile. This may be the case for early Mars whereby an Fe-Mg-silica-dominated solution resulted from leaching of rocks or sediments of basaltic composition. The Sheepbed member may have been leached preferentially of Mg, Fe, and SiO_2 by circulating meteoric fluids that preferentially dissolved olivine, and possibly some amount of glass and amorphous material, to form the Mg-Fe-saponite in the Sheepbed member [*Vaniman et al*., 2014]. The pH of the fluids that deposited the raised ridge minerals were likely circumneutral to slightly alkaline as Fe-rich saponites are most stable between pH 6 and 9 and Mg-rich clay minerals, most commonly form at pH greater than 8–9 [*Siffert and Wey*, 1962; *Léveillé et al*., 2002; *Tosca et al*., 2011; *Meunier*, 2005]. This is consistent with the findings for the proposed fluids that deposited the Sheepbed mudstone [*Grotzinger et al*., 2014 (J. Bridges, et al. Diagenesis and Clay Mineral Formation at Gale Crater, Mars, submitted to *Journal of Geophysical Research:* Planets, 2014)]. The lack of abundant soluble minerals points to a nonsaline fluid, though a brakish composition is possible (e.g., Bridges et al., submitted manuscript). However, we note that knowing the exact mineral composition (e.g., from CheMin X-Ray diffraction) of diagenetic features like these raised ridges would greatly increase our ability to derive paleoenvironmental conditions and better assess habitability.

In weathering profiles in mafic and ultramafic rocks on Earth (and possibly on Mars; see below), Mg-rich clay minerals are common in the deeper parts (e.g., saprolite) as Mg is more mobile than Fe or Al, which accumulate in leached layers above [e.g., *Veniale and van der Marel*, 1968; *Fontanaud and Meunier*, 1983; *Kodama et al*., 1988; *Ehlmann et al*., 2013]. The lower layers are thus enriched in the relatively mobile Mg, often as Mg-rich clay minerals. Assemblages of alteration minerals are often dominated by Fe-Mg smectites (nontronite and saponite), talc (or kerolite, a poorly ordered hydrated talc-like phase), serpentine, with oxides and possible zeolites, as well as Mg gels. However, the geological setting of Yellowknife Bay does not point to a weathering profile, and no significantly leached layer has been observed here [e.g., *Grotzinger et al*., 2014; *McLennan et al*., 2014]. In addition, at least one occurrence of raised ridges has been observed in the overlying Gillespie member [*Siebach et al*., 2014]. Nevertheless, it should be noted that changes in composition with depth can be small especially if the alteration is not extensive, as appears to be the case at Yellowknife Bay. *Fontanaud and Meunier* [1983] noted that chemical variations observed in a lherzolite rock having undergone weathering in a temperate climate can be relatively small, with Mg, Ca, and Na being only slightly enriched in the lower layers and Si, Al, Fe, and K enriched in upper, more leached, layers. They underline the importance of reactions at microsites, and they interpret these as open microsystems whereby the nature of mineral reactions is dictated by the amount of fluid entering the microsystem. The enrichment in MgO and depletion of immobile TiO_2 and Al_2O_3 in the raised ridges compared to the Sheepbed are perhaps consistent with some leaching of an upper unit, which may have been since deflated. The depletion of K_2O, on the other hand, in the raised ridges may instead be more related to crystal chemistry of the main phyllosilicates present, though we cannot verify this claim with the present data. Downward percolating fluids, enriched in Mg, could have precipitated an Mg-(Fe)-rich clay mineral due to temperature change (freezing) or more likely evaporation.

In recent years, phyllosilicates have been remotely detected at numerous locations on Mars, primarily by the High Resolution Imaging Science Experiment and Observatoire Martien pour l'étude de l'Eau, des Glaces et de l'Activité (OMEGA) spectroscopy instruments aboard the Mars Reconnaissance and Mars Express spacecraft, respectively [e.g., *Mustard et al*., 2008; *Carter et al*., 2010; *Ehlmann et al*., 2011, 2013; *Meunier et al*., 2012]. In fact, based on these observations, Fe/Mg smectites may be the most common phyllosilicates on Mars [*Ehlmann et al*., 2011]. Unfortunately, remote observations of Gale Crater are hindered by surface dust, and mineral identification for Yellowknife Bay are lacking. That being said, Fe/M smectites are expected to form during water/basalt interaction and diagenetic clays in veins have been explicitly predicted to form on

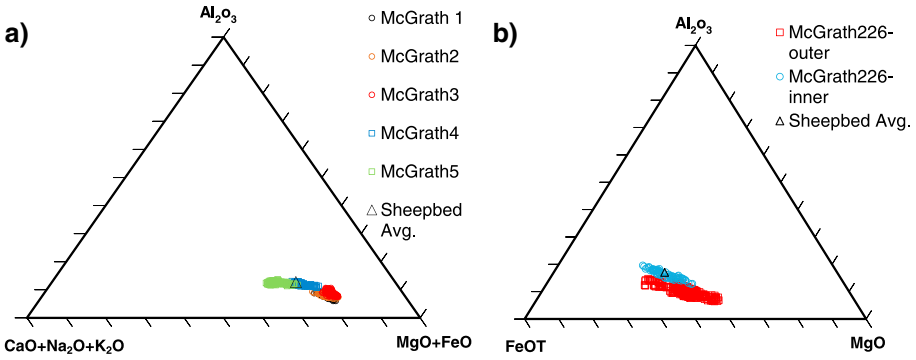

Figure 12. A-FM-CNK plot of single-shot data for (a) McGrath 5 (sol 234) 5 × 150 shot raster and (b) AFM plot of single-shot data for McGrath 4 (Sol 226) 20 × 30 shot raster. Locations 1–3 on the sol 234 raster are in the outermost layer and are distinct in composition from locations 4 and 5, which are in the innermost layer. These correspond to locations 1–10 and 14–16 (outermost layers) and locations 11–13 (innermost layer) in the sol 226 raster. In all cases, the first five shots of each analysis have been removed. The average composition of the Sheepbed mudstone is also plotted, and it can be seen to most closely match the composition of the innermost layer in McGrath.

Mars [*Ehlmann et al*., 2011]. In addition, the trend in composition observed for the raised ridges (e.g., Figure 12a) approximates closely the trend seen for the composition of Fe/Mg smectites (calculated from dust-removed modal mineralogy) in Nili Fossae and other cratered terrains (summarized in Figure 2 of *Ehlmann et al*. [2011, Figure 2]). This trend would appear to suggest that alteration took place in a system with low water/rock with relatively little compositional fractionation.

Volcanism, magmatism, and impact-induced hydrothermal activity have also been implicated in the formation of authigenic clay minerals on Mars, or their postdepositional alteration [e.g., *Ehlmann et al*., 2011; *Meunier et al*., 2012]. It is conceivable that smaller and younger impacts within Gale Crater may have led to localized, short-lived hydrothermal systems. While we have found no direct evidence for this based only on the compositional data from ChemCam and APXS, we cannot rule out this alternative explanation for the formation of the raised ridges. Despite this, given the mineralogy of the mudstone and the geological setting, we favor the low-temperature origin for the minerals in the raised ridges. This interpretation is supported by the geological context [*Grotzinger et al*., 2014], the geochemical and mineralogical evidence [*McLennan et al*., 2014; *Vaniman et al*., 2014], as well as thermochemical modeling of water-rock interaction in the Yellowknife Bay (Bridges et al., submitted manuscript).

After formation of the raised ridges, there was likely limited interaction with liquid water and especially limited or no interaction with acidic solutions. *Tosca and Knoll* [2009] noted than an abundance of Fe-Mg-smectites suggests the presence of immature sediments with no abundant interaction with liquid water postdeposition. Continued interaction with abundant liquid water could have led to leaching of the magnesium and alteration of the Mg-rich clay to more Fe-rich, nontronite-like phases, such as hisingerite [e.g., *Kohyama and Sudo*, 1975] or to chlorite through diagenesis [e.g., *Tosca and Knoll*, 2009]. Experimental results for dilute HCl leaching of saponite show removal of cations, initially mostly Mg (and followed by Fe) and production of free silica [*Vicente Rodriguez et al*., 1995]. No evidence for silica formation in the raised ridges was observed though we cannot rule this out completely. That being said, calcium- (and sodium-)rich saline fluids in desert lakes systems of the western U.S. do not promote significant changes in clay mineral composition, including smectites, during diagenesis [*Droste*, 1961]. Later-stage fluids were rich in Ca and S as Ca-S-rich veins are seen to crosscut raised ridges (Figures 3 and 4). However, these fluids did not react significantly with the raised ridges themselves likely due to low permeability of the host clay-rich mudstone and the ridges themselves.

4.5. Formation Scenario

We provide here a scenario of formation for the raised ridges in Yellowknife Bay. (1) Deposition and partial lithification of Sheepbed mudstone. (2) Cracking of Sheepbed mudstone. (3) Fluids flow through cracks. (4) Subaqueous deposition of initial MgO-rich, resistant cement along margins of cracks. Possible mechanisms may include partial dissolution of host Sheepbed mudstone, evaporation of partial freezing of fluids in cracks. (5) Infilling of remaining space with less resistant cement between outer layers of cement from fluid of

slightly different composition, notably with lesser MgO. (6) In some case, more than one less resistant inner cement layer is possible for a typical total of 3–4 distinct cement layers filling the cracks. (7) Deflation and exhumation of upper part of Sheepbed mudstone.

4.6. Future Investigations

Further refinements in data processing and quantitative estimates by the ChemCam team, continued systematic passive reflectance spectroscopy with both ChemCam and Mastcam, and additional CheMin and SAM-Evolved Gas Analysis analyses on related targets will help to further constrain the exact chemical composition and mineralogical makeup of these raised ridges, as well as other, possibly temporally or genetically related, diagenetic and sedimentary features. We also suggest that further work on the stability of Fe-Mg-smectites at Martian surface conditions, their use as pH and redox indicators, and their ability to preserve organic matter over geological time is needed. Continuing laboratory studies on coatings and multilayered fine-scale deposits will also lead to a better understanding of LIBS analyses of such complex multielement natural targets. Nevertheless, we have shown here that high spatial resolution three-dimensional chemical analyses of fine-scale features on Mars by ChemCam can reveal important details about past processes on Mars, including aqueous alteration and the deposition of secondary phases on a very small scale. The fact that ChemCam can make these observations remotely will continue to be an asset for mission operations, perhaps more so as *Curiosity* makes its way up valleys and between mesa-like features at the base of Mount Sharp, the primary science destination of the MSL mission. In addition, next-generation, laser-based spectroscopic instruments, possibly even combining both LIBS and Raman spectroscopy, will be a major asset on future landed missions.

5. Conclusions

Detailed and targeted probe-like analyses by ChemCam provide chemical compositions with unprecedented spatial resolution on Mars. The raised ridges in Yellowknife Bay show a composition that is distinct from the Sheepbed host mudstone and also show at least two distinct compositions, thus measuring, for the first time on Mars, a cement stratigraphy that records either an evolution in fluid composition or distinct fluid compositions over time. This is consistent with the interpretation of the raised ridges as being multilayered, isopachous fracture-filling precipitates. The raised ridges are the products of water-rock interaction, weathering, and early diagenesis. Mg- (Fe-)rich clay minerals likely record precipitation at near-neutral or slightly alkaline pH, which is consistent with previous interpretations for the Yellowknife Bay fluvial-lacustrine system [e.g., *Grotzinger et al*., 2014; *McLennan et al*., 2014]. Fluids would have initially precipitated Mg-Fe-phyllosilicates (and possibly some Fe oxides) in the raised ridges that may be similar to the clay minerals in the Sheepbed mudstone [*Vaniman et al*., 2014], possibly as a result of leaching of olivine or a basaltic precursor sediment. This was followed by a distinct episode of fracturing and vein filling with Ca sulfates at later stage [*Nachon et al*., 2014]. Chemical, mineralogical, and morphological evidence for multiple stages of fluid flow in the Sheepbed mudstone suggest that this location may have been habitable for an extended period of time.

Acknowledgments

The MSL mission is funded by NASA's Mars Program Office. R.J.L. received financial support from the Canadian Space Agency. The French contribution to ChemCam on MSL is supported by the Centre National d'Études Spatiales (CNES). We acknowledge the whole MSL team and JPL, in particular, for developing and leading this successful mission. We also thank the reviewers for their excellent comments, which greatly helped to improve the manuscript. The data reported in this paper are archived at the Planetary Data System, accessible at http://pds-geosciences.wustl.edu/missions/msl/index.htm.

References

Andrews, A. J. (1980), Saponite and celadonite in layer 2 basalts, DSDP Leg 37, *Contrib. Mineral. Petrol.*, *73*, 323–340.

Andrews, A. J., R. L. Barnett, B. A. E. MacClement, W. S. Fyfe, G. Morrison, N. D. MacRae, and J. Starkey (1977), Zeolite facies metamorphism, geochemistry and some aspects of trace element redistribution in altered basalts of DSDP, Leg 37. In DSDP Initial Reports, doi:10.2973/dsdp.proc.37.162.1977.

April, R. H., and D. M. Keller (1992), Saponite and vermiculite in amygdales of the Granby basaltic tuff, Connecticut Valley, *Clays Clay Min.*, *40*, 22–31.

Arvidson, R. E., et al. (2014), Ancient aqueous environments at Endeavour crater, Mars, *Science*, *343*, doi:10.1126/science.1248097.

Beaufort, D., and A. Meunier (1994), Saponite, corrensite and chlorite-saponite mixed-layers in the Sancerre-Couy deep drill-hole (France), *Clay Min.*, *29*, 47–61.

Bish, D. L., et al. (2013), X-ray diffraction results from Mars Science Laboratory: Mineralogy of Rocknest at Gale Crater, *Science*, *341*(6153), doi:10.1126/science.1238932.

Blaney, D. L., et al. (2014), Chemistry and texture of the rocks at Rocknest, Gale Crater: Evidence for sedimentary origin and diagenetic alteration, *J. Geophys. Res. Planets*, *119*(9), 2109–2131, doi:10.1002/2013JE004590.

Carter, J., F. Poulet, J.-P. Bibring, and S. Murchie (2010), Detection of hydrated silicates in crustal outcrops in the northern plains of Mars, *Science*, *328*(5986), doi:10.1126/science.1189013.

Changela, H. G., and J. C. Bridges (2010), Alteration assemblages in the nakhlites: Variation with depth on Mars, *Meteor. Planet. Sci.*, *45*, 1847–1867, doi:10.1111/j.1945-5100.2010.01123.x.

Clegg, S. M., E. Sklute, M. D. Dyar, J. E. Barefield, and R. C. Wiens (2009), Multivariate analysis of remote laser-induced breakdown spectroscopy spectra using partial least squares, principal component analysis, and related techniques, *Spectrochim. Acta, Part B*, *64*, 79–88, doi:10.1016/j.sab.2008.10.045.

Cousin, A. (2012), LIBS (Laser-Induced Breakdown Spectroscopy) pour l'exploration martienne, PhD thesis, Université de Toulouse 3 Paul Sabatier, Toulouse, France..

Cousin, A., O. Forni, S. Maurice, O. Gasnault, C. Fabre, V. Sautter, R. C. Wiens, and J. Mazoyer (2011), Laser induced breakdown spectroscopy library for the Martian environment, *Spectrochim. Acta*, *66*(11–12), 805–814, doi:10.1016/j.sab.2011.10.004.

Decarreau, A., N. Vigier, H. Palkova, S. Petit, P. Vieillard, and C. Fontaine (2012), Partitioning of lithium between smectite and solution: An experimental approach, *Geoch. Cosmoch. Acta*, *85*, 314–325.

Desprairies, A., P. Tremblay, and C. Laloy (1989), Secondary mineral assemblages in a volcanic sequence drilled during ODP Leg 104 in the Norwegian Sea, in *Proceedings of the Ocean Drilling Program, Scientific Results*, vol. 104, edited by Eldholm et al., pp. 397–409., Texas A&M University, College Station, Tex.

Droste, J. B. (1961), Clay mineral composition of sediments in some desert lakes in Nevada, California, and Oregon, *Science*, *133*, 1928.

Ehlmann, B. L., J. F. Mustard, S. L. Murchie, J.-P. Bibring, A. Meunier, A. A. Fraeman, and Y. Langevin (2011), Subsurface water and clay mineral formation during the early history of Mars, *Nature*, *479*, 53–60, doi:10.1038/nature10582.

Ehlmann, B. L., D. L. Bish, S. W. Ruff, and J. F. Mustard (2012), Mineralogy and chemistry of altered Icelandic basalts: Application to clay mineral detection and understanding aqueous environments on Mars, *J. Geophys. Res.*, *117*, E00J16, doi:10.1029/2012JE004156.

Ehlmann, B. L., G. Berger, N. Mangold, J. R. Michalski, D. C. Catling, S. W. Ruff, E. Chassefière, P. B. Niles, V. Chevrier, and F. Poulet (2013), Geochemical consequences of widespread clay mineral formation in Mars' ancient crust, *Space Sci. Rev.*, *174*, 329–364.

Fabre, C., S. Maurice, A. Cousin, R. C. Wiens, O. Forni, V. Sautter, and D. Guillaume (2011), Onboard calibration igneous targets for the Mars Science Laboratory Curiosity rover and the Chemistry Camera Laser-Induced Breakdown Spectroscopy instrument, *Spectrochim. Acta, Part B*, *66*, 280–289, doi:10.1016/j.sab.2011.03.012.

Fabre, C., et al. (2014), In situ calibration using univariate analyses based on the onboard ChemCam targets: First prediction of Martian rock and soil compositions, *Spectrochim. Acta, Part B*, *99*, 34–51.

Fontanaud, A., and A. Meunier (1983), Mineralogical facies of a weathered serpentinized lherzolite from the Pyrenees, France, *Clay Min.*, *18*, 77–88.

Garvie, L. A. J., and R. Metcalfe (1997), A vein occurrence of co-existing talc, saponite, and corrensite, Builth Wells, Wales, *Clay Min.*, *32*, 223–240.

Grauby, O., S. Petit, A. Decarreau, and A. Baronnet (1994), The nontronite-saponite series: An experimental approach, *Eur. J. Mineral.*, *6*, 99–112.

Grotzinger, J. P., et al. (2014), A habitable fluvio-lacustrine environment at Yellowknife Bay, Gale Crater, Mars, *Science*, *343*(6169), doi:10.1126/science.1242777.

Hagerty, J. J., and H. E. Newsom (2003), Hydrothermal alteration at the Lonar Lake impact structure, India: Implications for impact cratering on Mars, *Met. Planet. Sci.*, *38*, 365–381.

Kauffman, J., H. S. Cander, L. D. Daniels, and W. J. Meyers (1988), Calcite cement stratigraphy and cementation history of the Burlington-Keokuk Formation (Mississippian), Illinois and Missouri, *J. Sed. Pet.*, *58*, 312–326.

Kim, T., B. T. Nguyen, V. Minassian, and C. T. Lin (2007), Paints and coatings monitored by laser-induced breakdown spectroscopy, *J. Coat. Tech. Res.*, *4*, 41–253.

Knoll, A. H., et al. (2008), Veneers, rinds, and fracture fills: Relatively late alteration of sedimentary rocks at Meridiani Planum, Mars, *J. Geophys. Res.*, *113*, E06S16, doi:10.1029/2007JE002949.

Kodama, H., C. R. De Kimpe, and D. Dejou (1988), Ferrian saponite in a gabbro saprolite at Mont Mégantic, Québec, *Clays Clay Min.*, *36*, 102–120.

Kohyama, N., and T. Sudo (1975), Hisingerite occurring as a weathering product of iron-rich saponite, *Clays Clay Min.*, *23*, 215–218.

Langevin, Y., B. Gondet, S. Le Mouelic, O. Gasnault, K. Herkenhoff, D. Blaney, S. Maurice, R. Wiens, and the MSL Science Team (2013), Processing approaches for optimal science exploitation of the ChemCam Remote Microscopic Imager (RMI) during the first 90 days of Curiosity operations, *Lunar Planet. Sci., XLIV*, 1227.

Lanza, N. L., S. M. Clegg, R. C. Wiens, R. E. McInroy, H. Newson, and M. D. Deans (2012), Examining natural rock varnish and weathering rinds with laser-induced breakdown spectroscopy for application to ChemCam on Mars, *App. Optics*, *51*, B74–B82, doi:10.1364/AO.51.000B74.

Lanza, N. L., et al. (2014a), Manganese trends with depth on rock surfaces in Gale Crater, Mars, *Lunar Planet. Sci., XLV*, 2599.

Lanza, N. L., et al. (2014b), Understanding the signature of rock coatings in laser-induced breakdown spectroscopy data, *Icarus*, 10.1029/2012JE004156.

Le Mouélic, S., et al. (2014), The ChemCam Remote Micro-Imager at Gale crater: Review of the first year of operations on Mars, Icarus, in press.

Léveillé, R. J., F. J. Longstaffe, and W. S. Fyfe (2002), Kerolite in carbonate-rich speleothems and microbial deposits from basaltic sea caves, Kauai, Hawaii, *Clays Clay Min.*, *50*, 514–524.

Madamba, M. C., W. M. Mullett, S. Debnath, and E. Kwong (2007), Characterization of tablet film coatings using a laser-induced breakdown spectroscopic technique, *AAPS Pharm. Sci. Tech.*, *8*, 184–190.

Maurice, S., et al. (2012), The ChemCam instrument suite on the Mars Science Laboratory (MSL) rover: Science objectives and mast unit description, *Space Sci. Rev.*, *170*, 95–166.

McLennan, S. M., et al. (2005), Provenance and diagenesis of the evaporite-bearing Burns formation, Meridiani Planum, Mars, *Earth Planet. Sci. Lett.*, *240*(1), 95–121, doi:10.1016/j.epsl.2005.09.041.

McLennan, S. M., et al. (2014), Elemental geochemistry of sedimentary rocks in Yellowknife Bay, Gale Crater, Mars, *Science*, *343*(6169), doi:10.1126/science.1244734.

Meslin, P.-Y., et al. (2013), Soil diversity and hydration as observed by ChemCam at Gale Crater, Mars, *Science*, *341*, doi:10.1126/science.1238670.

Meunier, A. (2005), *Clays*, 472 pp., Springer-Verlag, Berlin.

Meunier, A., S. Petit, B. L. Ehlmann, P. Dudoignon, F. Westall, A. Mas, A. El Albani, and E. Ferrage (2012), Magmatic precipitation as a possible origin of Noachian clays on Mars, *Nat. Geosci.*, *5*, 739–743, doi:10.1038/ngeo1572.

Ming, D. W., et al. (2014), Volatile and organic compositions of sedimentary rocks in Yellowknife Bay, Gale Crater, Mars, *Science*, *343*(6169), doi:10.1126/science.1245267.

Morris, R. V., et al. (2000), Mineralogy, composition, and alteration of Mars Pathfinder rocks and soils: Evidence from multispectral, elemental, and magnetic data on terrestrial analogue, SNC meteorite, and Pathfinder samples, *J. Geophys. Res.*, *105*(E1), 1757–1817, doi:10.1029/1999JE001059.

Mustard, J. F., et al. (2008), Hydrated silicate minerals on Mars observed by the Mars Reconnaissance Orbiter CRISM instrument, *Nature*, *454*, 305–309, doi:10.1038/nature07097.

Nachon, M., et al. (2014), Calcium sulfate veins characterized by ChemCam/Curiosity at Gale crater, Mars, *J. Geophys. Res. Planets*, *119*, 1991–2016, doi:10.1002/2013JE004588.
Novotny, K., T. Vaculovic, M. Galiova, V. Otruba, V. Kanicky, J. Kaiser, M. Liska, O. Samek, R. Malina, and K. Palenikova (2007), The use of zinc and iron emission lines in the depth profile analysis of zinc-coated steel, *App. Surf. Sci.*, *253*, 3834–3842.
Ollila, A. O., et al. (2014), Trace element geochemistry (Li, Ba, Sr, and Rb) using Curiosity's ChemCam: Early results for Gale Crater from Bradbury Landing Site to Rocknest, *J. Geophys. Res. Planets*, *118*, 1–31, doi:10.1002/2013JE004517.
Rampe, E. B., et al. (2014), Characterizing the phyllosilicate component of the Sheepbed Mudstone in Gale Crater, Mars using laboratory XRD and EGA. Lunar and Planetary Science Conference, Abstract XXXX.
Schröder, S., et al. (2014), Hydrogen detection with ChemCam at Gale crater, *Icarus*, doi:10.1016/j.icarus.2014.08.029.
Siebach, K. L., J. P. Grotzinger, L. C. Kah, K. M. Stack, M. Malin, R. Léveillé, and D. Y. Sumner (2014), Subaqueous shrinkage cracks in the Sheepbed mudstone: Implications for early fluid diagenesis, Gale crater, *Mars, J. Geophys. Res. Planets*, *119*(7), 1597–1613 doi:10.1002/2014JE004623.
Siffert, B., and R. Wey (1962), Synthèse dune sépiolite a température ordinaire, *C. R. Acad. Sci.*, *254*(8), 1460–1462.
Squyres, S. W., et al. (2004), In situ evidence for an ancient aqueous environment at Meridiani Planum, Mars, *Science*, *306*, 1709–1714, doi:10.1126/science.1104559.
Stack, K. M., et al. (2014), Diagenetic origin of nodules in the Sheepbed member, Yellowknife Bay formation, Gale crater, Mars, *J. Geophys. Res. Planets*, *119*(7), 1637–1664, doi:10.1002/2014JE004617.
Squyres, S. W., et al. (2012), Ancient impact and aqueous processes at Endeavour crater, Mars, *Science*, *336*, 570–576, doi:10.1126/science.1220476.
Starkey, H. C. (1982), *The Role of Clays in Fixing Lithium*, 11 pp., U.S. Geol. Surv. Bull., 1278-F, Wash.
St-Onge, L., and M. Sabsabi (2000), Towards quantitative depth-profile analysis using laser-induced plasma spectroscopy: Investigation of galvannealed coatings on steel, *Spectrochim. Acta, Part B*, *55*, 299–308.
Tosca, N. J., and A. H. Knoll (2009), Juvenile chemical sediments and the long term persistence of water at the surface of Mars, *Earth Planet. Sci. Lett.*, *286*, 379–386.
Tosca, N. J., F. A. Macdonald, J. V. Strauss, D. T. Johnston, and A. H. Knoll (2011), Sedimentary talc in Neoproterozoic carbonate successions, *Earth Plan. Sci. Lett.*, *306*, 11–22.
Treiman, A. H., R. A. Barrett, and J. L. Gooding (1993), Preterrestrial aqueous alteration of the Lafayette (SNC) meteorite, *Meteoritics*, *28*, 86–97.
Treiman, A. H., et al. (2014), Ferrian saponite from the Santa Monica mountains (California, U.S.A., Earth): Characterization as an analog for clay minerals on Mars with application to Yellowknife Bay in Gale Crater, *Am. Mineralog.*, *99*, doi:10.2138/am-2014-4763.
Vadillo, J. M., and J. J. Laserna (1997), Depth-resolved analysis of multilayered samples by laser-induced breakdown spectrometry, *J. Anal. Atomic Spec.*, *12*, 859–862.
Vaniman, D. T., et al. (2014), Mineralogy of a mudstone at Yellowknife Bay, Gale Crater, Mars, *Science*, doi:10.1126/science.1243480.
Vaniman, D., M. D. Dyar, R. Wiens, A. Ollila, N. Lanza, J. Lasue, J. M. Rhodes, S. Clegg, and H. Newsom (2012), Ceramic ChemCam calibration targets on Mars Science Laboratory, *Space Sci. Rev.*, *170*, 229–255, doi:10.1007/s11214-012-9886-0.
Veniale, F., and H. W. Van der Marel (1968), A regular talc-saponite mixed-layer mineral from Ferriere, Nure Valley (Piacenza Province, Italy), *Contrib. Min. Petr.*, *17*, 237–254.
Vicente Rodriguez, M. A., J. D. López Gonzáilez, and M. A. Bafiares-Mufioz (1995), Preparation of microporous solids by acid treatment of a saponite, *Micropor. Matter*, *4*, 251–264.
Wiens, C. R., et al. (2012), The ChemCam instrument suite on the Mars Science Laboratory (MSL) rover: Body unit and combined system tests, *Space Sci. Rev.*, *170*, 167–227.
Wiens, R. C., et al. (2013), Pre-flight calibration and initial data processing for the ChemCam laser-induced breakdown spectroscopy instrument on the Mars Science Laboratory rover, *Spectrochim. Acta, Part B*, *82*, 1–27, doi:10.1016/j.sab.2013.02.003.
Williams, R. M. E., et al. (2013), Martian fluvial conglomerates at Gale Crater, *Science*, *340*(6136), 1068–1072, doi:10.1126/science.1237317.
Wolela, A. M., and E. H. Gierlowski-Jordesch (2007), Diagenetic history of fluvial and lacustrine sandstones of the Hartford Basin (Triassic-Jurassic), Newark Supergroup, USA, *Sed. Geol.*, *197*, 99–126.
Yamin Ali, M. (1995), Carbonate cement stratigraphy and timing of diagenesis in a Miocene mixed carbonate-clastic sequence, offshore Sabah, Malaysia: Constraints from cathodoluminescence, geochemistry, and isotope studies, *Sed. Geol.*, *99*, 191–214.